Journal of The Electrochemical Society, **152** (12) A2357-A2363 (2005)
0013-4651/2005/152(12)/A2357/7/$7.00 © The Electrochemical Society, Inc.

Mixed Phase Pt-Ru Catalyst for Direct Methanol Fuel Cell Anode by Flame Aerosol Synthesis

D. Chakraborty,[a,*] H. Bischoff,[a] I. Chorkendorff,[a,b] and T. Johannessen[a,,z]**

[a]*Interdisciplinary Research Center for Catalysis (ICAT), Department of Chemical Engineering, and* [b]*Department of Physics, Technical University of Denmark, DK-2800 Kgs. Lyngby, Denmark*

A spray-flame aerosol catalyzation technique was studied for producing Pt-Ru anode electrodes for the direct methanol fuel cell. Catalysts were produced as aerosol nanoparticles in a spray-flame reactor and deposited directly as a thin layer on the gas diffusion layer. The as-prepared catalyst was found to be a mixture of nanocrystalline, mostly unalloyed Pt and an amorphous phase mostly of Ru and to a lesser extent of Pt oxides on top of the crystalline phase. The flame-produced Pt1Ru1 demonstrated similar onset potential but ~60% higher activity compared to commercially available Pt1Ru1/Vulcan carbon. The kinetics of methanol oxidation on the mixed phase catalyst was also explored by electrochemical impedance spectroscopy.
 [DOI: 10.1149/1.2109547]

Manuscript submitted January 20, 2005; revised manuscript received August 6, 2005. Available electronically October 26, 2005.

The direct methanol fuel cell (DMFC) uses methanol as fuel and has significant advantages over hydrogen-fed proton exchange membrane (PEM) fuel cells in mobile applications in terms of fuel storage and supply.[1] However, one of the main challenges of making DMFCs commercially feasible is to improve the slow reaction kinetics of the methanol oxidation reaction at the anode. There is an initial activation overpotential of some 0.2–0.55 V, depending on the catalyst and operating conditions, required to oxidize methanol anodically at an appreciable rate. At least some of this initiating overpotential is kinetic in nature and could be reduced by suitable catalysts at the anode.[2] Another critical issue of DMFC is the thickness of the anode catalyst layer. A thick catalyst layer increases the ohmic resistance as well as mass-transfer resistance for methanol. Therefore, to improve the DMFC anode performance it is necessary to investigate new catalytic materials for methanol electro-oxidation as well as alternative methods for catalyst preparation and membrane electrode assembly (MEA) fabrication.

In acidic medium, only Pt or Pt-based catalysts have been found to show acceptable activity and stability.[3] Platinum dehydrogenates methanol producing possibly adsorbed CO and other surface species which potentially block the Pt sites. To regenerate the Pt sites for further methanol oxidation at the DMFC operating range of interest ($<$0.5 V), Pt needs to be promoted by other metals. A promoter could change the electronic structure of Pt so that surface-blocking species are less strongly adsorbed, reducing the coverage and thereby the blocking effect. This effect is known as the ligand effect.[4] A promoter could also activate water at lower potentials than Pt to accelerate the oxidation and removal of surface-blocking species. This is known as a bifunctional mechanism.[5] Any enhancement of performance due to the promoter is related to either one or both of the two above-mentioned processes.[6] Although several other additives have been studied, and some ternary and quaternary alloys have been shown to possess higher activity than Pt-Ru as DMFC anode catalyst,[7] Pt-Ru is still the most studied catalyst for DMFC anodes.

It is still a matter of debate whether Ru should be present in the catalyst alloyed with Pt or as RuO_x for the best catalytic performance. Gottesfeld et al. have observed that Pt-Ru catalysts with stronger metallic character exhibit higher electrocatalytic activity for methanol oxidation than the more oxidic ones.[8,9] However, they concluded that the presence of RuO_x is beneficial for protonic conductivity within the catalyst layer.[9] Sirk et al. also have observed that the commercially available Johnson-Matthey Pt-Ru methanol oxidation catalyst has higher activity when it is reduced in hydrogen compared to the activity shown by the as-received catalyst.[10] Rolison et al. have hypothesized that the alloying of Pt with Ru is not the way to improve catalyst performance for methanol electro-oxidation.[11,12] They observed that Pt^0Ru^0 has orders of magnitude less electrocatalytically active for the reaction than the mixture of metallic Pt and hydrous ruthenium oxides (RuO_xH_y). They have also concluded that the ubiquitous way of confirming alloying from the X-ray diffraction (XRD) pattern is not applicable for the high-surface-area mixed-phase Pt-Ru methanol oxidation catalyst, and so the mixtures of metallic Pt and amorphous RuO_xH_y have been wrongly identified as Pt-Ru alloys. Also, it has been reported that the record high performance of a DMFC at the Los Alamos National Laboratory was obtained by using Pt-RuO_x as the anode catalyst.[13]

The conventional methods of preparing fuel cell electrodes consist of synthesis of catalysts, either supported or unsupported, and applying the catalyst as a thin layer on the electrolyte membrane or GDL, by painting or spraying.[5,7-9,14,15] However, there have also been a few attempts of directly loading the catalyst layer on the membrane and/or on the gas diffusion layer (GDL) by sputter deposition[16-20] and electrochemically.[21] Direct deposition could be an important step for streamlining the MEA fabrication process desirable for commercial production of fuel cells. Recently, we have established a one-step method for preparation of the DMFC Pt-Ru anode catalyst layer by using flame-spray pyrolysis. In this process, after dissolving Pt and Ru precursors in appropriate solvents, the solution is sprayed through a nozzle to produce micrometer-sized droplets which burn out in a flame, resulting in metal atoms and/or metal oxide molecules in the gas phase. Hereafter, clusters immediately nucleate and grow to nanosized particles by coagulation and/or surface reaction and sintering.[22] The mechanism of the particle formation process in the gas phase ensures intimate mixing of the product components.

As described in the Experimental section, the flame aerosol synthesis method averts the tedious and cumbersome step of catalyst ink painting in MEA preparation. Platinum and Pt-Ru with atomic ratios of 3:1 and 1:1 (Pt:Ru) were prepared and deposited on the GDL from the gas phase. In this article, the catalysts are designated by writing the atomic ratio after the element, i.e., Pt3Ru1 means that the nominal Pt to Ru atomic ratio of the deposit is 3:1. The deposits have been characterized by XRD, X-ray photoelectron spectroscopy (XPS), scanning electron microscopy (SEM), X-ray energy-dispersive spectroscopy (EDS), and transmission electron microscopy (TEM). After fabrication of the MEA, the catalysts have been electrochemically tested for methanol electro-oxidation and the performance has been compared with that of commercially available E-TEK Pt1Ru1/Vulcan carbon anode. The methanol oxidation kinetics has also been investigated by electrochemical impedance spectroscopy (EIS).

Experimental

Catalyst preparation and deposition.— The metal precursors used were ruthenium(III) acetylacetonate [$Ru(acac)_3$, Fluka, purity

* Electrochemical Society Student Member.
** Electrochemical Society Active Member.
z E-mail: tj@kt.dtu.dk

$\geqslant$97%] and platinum(II) acetylacetonate [Pt(acac)$_2$, Aldrich Chemical Co., 97% purity]. The solvent was a 4:1 volume ratio mixture of isooctane (Fluka, purity 99%) and tetrahydrofuran (Sigma, purity 99%). In all the stock solutions, the concentration of Pt(acac)$_2$ was kept constant while the concentration of Ru(acac)$_3$ was varied according to the required catalyst composition. The following solutions were prepared: 40 mg of Pt(acac)$_2$ in 100 mL of the solvent for Pt, 40 mg of Pt(acac)$_2$ and Ru(acac)$_3$ each with 100 mL of the solvent for Pt1Ru1, and 40 mg of Pt(acac)$_2$ and 13.3 mg of Ru(acac)$_3$ with 100 mL of the solvent for Pt3Ru1. The solution was pumped by using a syringe pump (IVAC P6000) through a gas-assisted nozzle to spray the precursor solution to the flame zone as small droplets. The nozzle consisted of a capillary tube o.d. 0.9 mm (i.d. 0.6 mm), which is situated in an opening of 1.4-mm diam, creating an annular space of 0.9 mm^2. The design of the nozzle is similar to the one used by Mädler et al.[23] The precursor solution was passed through the capillary tube at 30 mL/h and oxygen, as both the dispersion and oxidation gas, was introduced through the annulus at 2.2 L/min. The spray aerosol was ignited by eight hydrogen-fed supporting flames made by horizontal injection through eight equidistant holes drilled in a hollow metal ring placed around the aerosol jet. Cold air, provided from a water-cooled quenching ring, was used to quench the aerosol coming out of the flame.[24] The quenching helps decrease the average particle size by suddenly lowering the temperature and thus decreasing the rate of sintering. The product particles were collected directly on the GDL (Toray TGPH090) by withdrawing the nanoparticle aerosol from the flame through it by using a gas-ejector vacuum pump (PIAB Classic). Here, the GDL was, in principle, applied as a catalyst nanoparticle filter.

Physical and chemical characterization.— The XRD patterns were obtained from the catalyzed GDLs with a Philips diffractometer with a Cu Kα radiation source and a nickel filter. The scans were performed over a 2θ range of 20–95° with a scan step of 0.05° and acquisition time of 4 s. The crystalline sizes and peak angles were determined using Xfit[25] with a fundamental parameter fitting approach and using the entire XRD pattern (20–95°). An external Si standard was used to correct the sample displacement errors.[15] The Si powder (Aldrich) was sprinkled carefully on the catalyzed layer before taking the XRD pattern. The lattice parameters for the nanocrystalline phase were calculated from the line position of Pt(111) by using the following formula

$$a_{\mathrm{fcc}} = \sqrt{3}\lambda/(2 \sin \theta) \quad [1]$$

where λ = 1.54056 Å, the wavelength of radiation used, and θ is the Bragg angle for the measured peak.

The SEM and EDS experiments were done by LEO SUPRA50. For EDS, 32 different nonoverlapping areas with a diameter of 1 μm on the Pt1Ru1 catalyst layer were investigated with an electron-beam of 20 keV accelerating voltage for elemental information and the average was taken as the catalyst layer composition. With this accelerating voltage, the electron could penetrate to a depth on the order of 1.0 μm.[26] The TEM images were obtained with JEOL 3000F. The sample was prepared by scraping off the deposits from the GDL and suspending in ethanol. This suspension was added as a droplet on the holey carbon grid.

XPS of the catalyzed face of GDLs for various samples were recorded on a Phi 550 spectrometer by employing a Mg Kα source operating at 200 W. All the XPS spectra were obtained with pass energy of 50 eV for wide scans and 25 eV for individual elements. The samples were introduced into the spectrometer using a separate fast-entry chamber. The ratio between Pt and Ru atoms at the surface layer, $[\mathrm{Pt}]_{\mathrm{surf}}/[\mathrm{Ru}]_{\mathrm{surf}}$, were estimated from the following equation[27]

$$[\mathrm{Pt}]_{\mathrm{surf}}/[\mathrm{Ru}]_{\mathrm{surf}} = (I_{\mathrm{Pt}}/S_{\mathrm{Pt}})/(I_{\mathrm{Ru}}/S_{\mathrm{Ru}}) \quad [2]$$

where S_i is the atomic sensitivity factor and I_i is the area under the core-level peak considered.

Electrochemical experiments.— The flame-aerosol-produced anode with a Pt1Ru1 catalyst layer and a total metal loading of $\sim$1.5 mg/cm^2 was soaked with 0.1 mL of 5% Nafion in lower aliphatic alcohol solution (Aldrich Chemical Co.) and dried in open air for 30 min and at 80°C for 1 h in an oven to remove the alcohol. The anode from carbon-supported Pt–Ru (used for comparison) and all the cathodes was prepared by the following procedure. Commercially available PtRU/Vulcan carbon catalysts having 1:1 atomic ratio and 10 wt % total metal loading was obtained from E-TEK, Inc. Anode catalysts were applied to the MEAs at a total metal loading of $\sim$1.5 mg/cm^2. The total metal loading of the cathode catalyst was $\sim$2 mg/cm^2 (20% Pt/Vulcan carbon, E-TEK). The catalyst samples were ultrasonically mixed for 20 min in a clean bottle with 0.1 mL of 5% Nafion in lower aliphatic alcohol solution and deionized water. Isopropyl alcohol in water was added as a diluent to form a well-mixed catalyst ink. The catalyst inks were then brushed onto the GDL. Once all catalysts had been deposited, the electrodes were dried for 30 min in air at room temperature and for 1 h in an oven at 80°C. Similar cathodes were used with both flame-prepared anode and conventionally made anode with E-TEK catalyst. To prepare the MEAs, Nafion 112 polymer electrolyte membranes had been sandwiched between anode and cathode electrodes and pressed at $\sim$140°C and 200 bars for 5 min. All the MEAs prepared had circular electrodes with a diameter of 2 cm.

The MEAs were placed between two graphite bipolar plates (Sigracet) which had machined flow channels with serpentine flow pattern, capable of accommodating electrodes of maximum 3.14 cm^2 in a homemade single cell (designed by IRD Fuel Cells A/S). The sides of the stainless steel current collectors, which were not contacting the bipolar plates, had serpentine channels. The channels were separated from the water-filled chambers by Nafion membranes. Gas streams were humidified by passing the gases through the channels. When methanol was fed at the anode, the water chamber at the anode side was emptied. For all the experiments reported in the article where methanol was fed to the anode, the concentration of the solution was 1 mol/L and the flow rate was 1 mL/min. For cell polarization measurements, the cathode was fed with humidified O_2 at a cylinder back pressure of 2 bars and a flow rate of 80 sccm. For anode polarization and EIS, the cathode was fed with humidified H_2 at a rate of 5 sccm and functioned as a dynamic hydrogen electrode (DHE).[8,28-30] The cathode was also the counter electrode. The anode was fed with methanol and functioned as working electrode. The scans for polarization measurements were performed from 0 to 0.8 V vs DHE at 1 mV/s. For EIS, the frequency range was from 1 kHz to 50 mHz and the measurements were done at different dc potentials vs DHE. The amplitude of the sinusoidal voltage signal used was 10 mV. The conditioning of the MEAs was started by flowing overnight humidified H_2 and humidified Ar at the anode and cathode, respectively, at room temperature. Then the cell was run as a H_2/O_2 fuel cell at 90°C for 1 h with humidified H_2 at the anode.[8] After that H_2 at the anode was replaced with 1.0 M methanol and the cell voltage was cycled continuously for 1 h between open circuit to 0.8 V at a scan rate of 50 mV/s to finish the conditioning. Before taking any measurement, the cell was cycled between 0 and 0.8 V at 50 mV/s until reproducibility was established. All the electrochemical measurements were performed with the potentiostat PARSTAT 2273.

Results and Discussion

The SEM image shows the morphology of the deposits on the GDL (Fig. 1). The deposit seems to be porous and fluffy. This is possibly the result of the primary particles sticking together rather than sintering to form bigger single particles. The porous nature of the deposits is thought to be advantageous for transport of materials in and out of the agglomerates. The TEM image shows the highly crystalline metallic particles on the carbon grid (Fig. 2). The lattice spacing of 2.23 and 2 Å representing (111) and (002) planes, respectively, of the face-centered cubic (fcc) crystal of Pt are observed. No crystalline phase of either Ru or RuO_2 could be detected from the

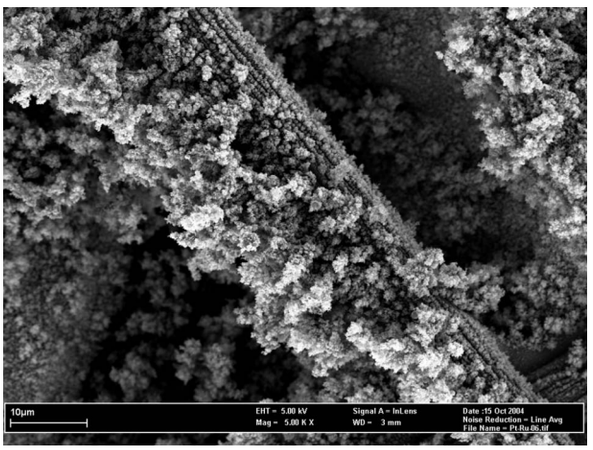

Figure 1. SEM image of the flame-produced Pt-Ru deposited on GDL.

d-spacing of the crystallites. Figure 3 shows the XRD patterns of the flame-synthesized Pt, Pt3Ru1, and Pt1Ru1 catalyzed layers on GDL. For all the patterns shown, the five characteristic peaks of the fcc crystalline structure of Pt, namely, the (111), (200), (220), (311), and (222) could be seen. However, no significant peak shift was observed with increasing Ru content in the sample. The lattice parameters (a_{fcc}) show an insignificant gradual decrease with increasing Ru content compared to the arc-melted Pt-Ru alloy reported by Gasteiger et al.[31] (Fig. 4). For the arc-melted alloys, the lattice parameter decreases linearly with increasing Ru content, consistent with the smaller size of Ru atoms compared to Pt. Also shown in the figure are the reported a_{fcc} values for the Johnson-Matthey unsupported Pt-Ru catalyst[15] and the high-surface-area unsupported Pt-Ru catalyst prepared by rapid borohydride reduction of aqueous metal salts.[7] The a_{fcc} values for high-surface-area Pt1Ru1 is higher than that of arc-melted Pt-Ru. However, the decrease in a_{fcc} from pure Pt to Pt1Ru1 for flame-synthesized catalyst is almost an order of magnitude less than that obtained for commercial Johnson-Matthey Pt1Ru1,[15] implying that in our catalyst the nanocrystalline phase consists mostly of Pt. The absence of any other crystalline phase leads us to envisage the flame-prepared catalysts as a mixture of a crystalline phase consisting predominately of Pt and one or more amorphous phases consisting of mainly Ru as metallic or oxidic states. The particle size of the crystalline phase of Pt1Ru1, as determined from XRD peak broadening, is 10.3 ± 0.3 nm. The peak at ~54° is a carbon peak coming from the TGPH 090 support and it has been confirmed by performing XRD on a blank TGPH 090 (figure not shown).

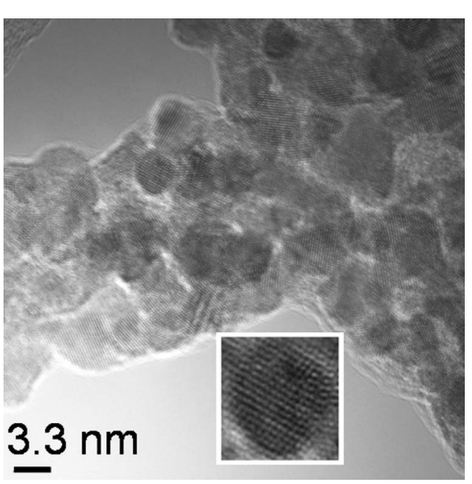

Figure 2. TEM image of the flame-produced nanocomposites on holey carbon grid. The insert shows the crystalline plane of a nanoparticle. Note that the scale bar is for the main figure and not the insert.

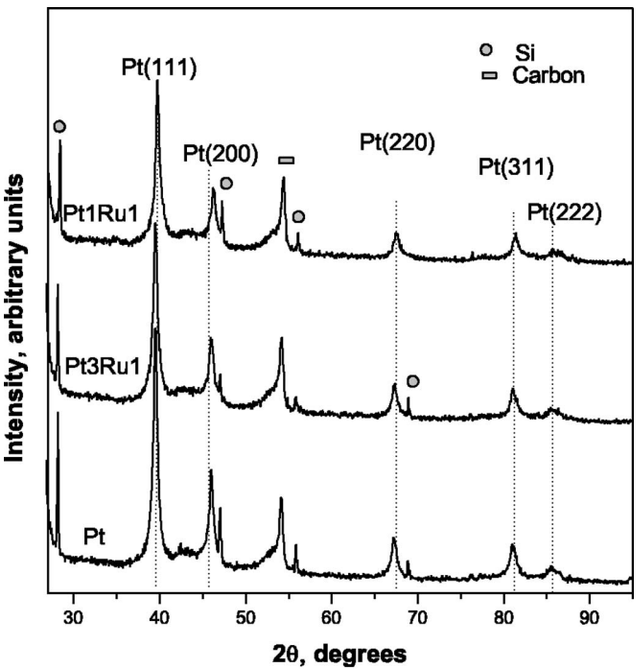

Figure 3. XRD patterns for catalyzed layers of Pt, Pt3Ru1, and Pt1Ru1 on GDL. Si powder sprinkled on the catalyst layers served as an external standard for correcting sample displacement errors. The spectra were collected between the 2θ values of 20 and 95°; however, a zoomed-in window of 25–95° is shown.

Overall X-ray photoemission spectrum of the TGPH 090 carbon support and different catalysts are shown in Fig. 5. Peaks of Pt 4f, Pt

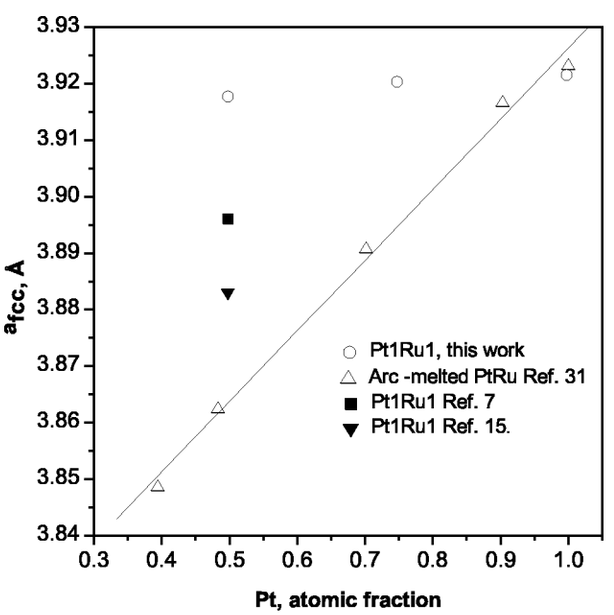

Figure 4. Comparison of lattice parameters of the fcc phase of flame-synthesized catalysts with that of the literature reported high-surface-area catalysts (Ref. 7 and Ref. 15) and arc-melted Pt-Ru alloys (Ref. 31).

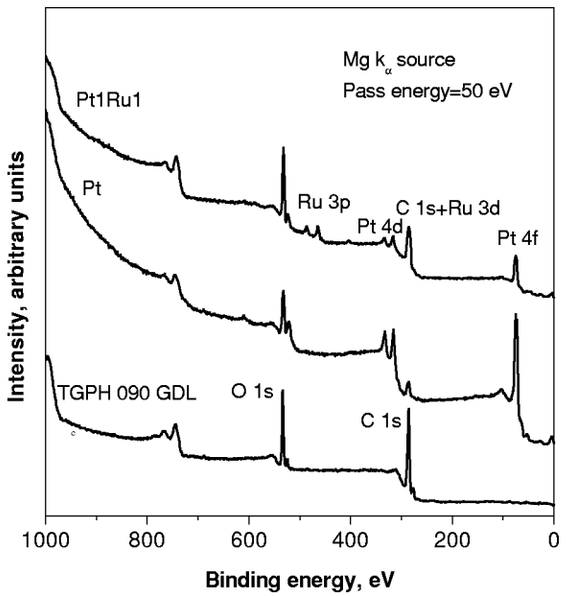

Figure 5. Overall XPS spectra of the TGPH 090 GDL, Pt, and Pt1Ru1 catalyst layer on GDL.

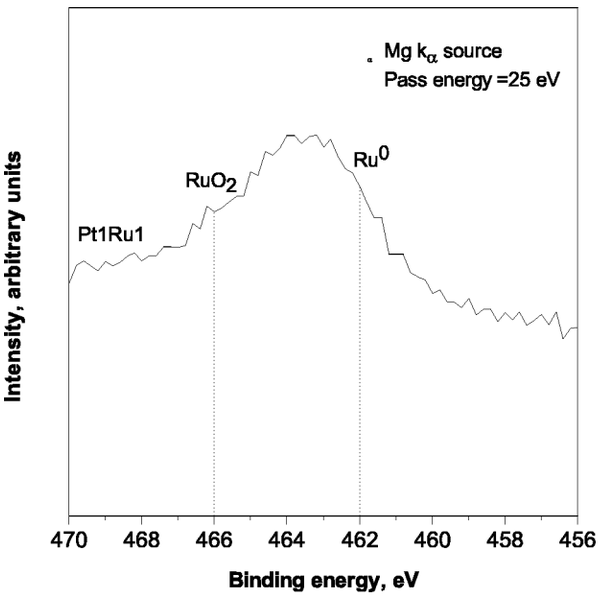

Figure 7. The XPS spectra for Ru $3p_{3/2}$ core region of Pt1Ru1 catalyst layer on GDL. The vertical lines are the values reported in literature for the binding energies of different oxidation states of Ru.

4d, C 1s, and O1s are observed for the Pt catalyst layer. All the peaks present in the Pt catalyst layer could also be seen for Pt1Ru1. The peaks of Ru 3d overlapped with C 1s, and Ru 3p peaks are also observed. In Fig. 6, the Pt 4f core-level spectrum of the Pt and Pt1Ru1 catalyst layers on GDL are shown. The vertical lines at 71.0, 72.4, and 73.8 eV are the binding energies reported for the $4f_{7/2}$ peak of Pt, $Pt(OH)_2$, and PtO, respectively.[32] Because of the lack of information about the exact nature of the compounds formed, no deconvolution and curve-fitting has been done. However, from Fig. 6, it may be deduced that oxidized Pt is present in relatively large amount in the Pt1Ru1 sample compared to the Pt sample. A significant enhancement of the amount of Pt-O species with the presence

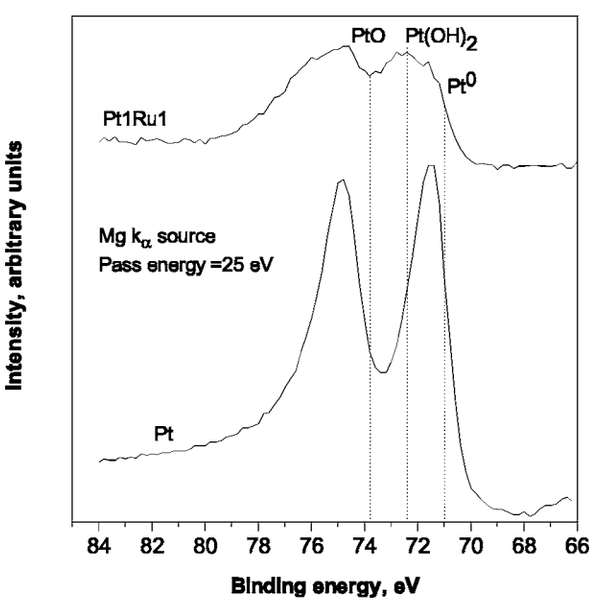

Figure 6. The XPS spectra for the Pt 4f core region of Pt and Pt1Ru1 catalyst layers on GDL. The vertical lines are the literature reported values for the binding energies of different oxidation states of Pt.

of Ru has been reported in the literature for Pt-Ru DMFC anode catalyst. The observation has been attributed to the increase of the coverage of Pt-Ru surfaces by oxy-species due to Ru.[3,33-35] However, no crystalline Pt-oxide phase in our catalyst is detected from XRD, possibly indicating that Pt oxides are present mostly at the surface in an amorphous phase. Figure 7 shows the Ru $3p_{3/2}$ peak for the Pt1R1 sample. The vertical lines at 462 and 466 eV are the binding energies reported for metallic Ru and rutile RuO_2.[36] It could be deduced that the bulk of the Ru exists at oxidation states between metallic Ru and Ru^{+4}. The surface concentration of Pt and Ru estimated from the intensities of Pt 4f and Ru $3p_{3/2}$ (atomic sensitivity factors of 4.4 and 1.30, respectively[37]) peaks by using Eq. 2 gives a Pt atomic fraction of 0.48. However, the average of the Pt atomic fraction determined from EDS is 0.58 ± 0.03. Considering the fact that XPS signals mainly come from the surface and EDS signals primarily come from the bulk, the difference between the Pt atomic fraction determined from XPS and EDS could be rationalized by postulating a thin amorphous surface layer consisting of Pt-Ru oxides on top of the nanocrystalline Pt fcc phase.

Figure 8 shows the Tafel slopes (b) for methanol oxidation by Pt1Ru1 at different temperatures. The overpotential data is corrected for iR losses while the ohmic resistances at different temperatures have been determined from ac impedance experiments. The Tafel slope decreases from 135 mV/d at 25°C to 95 mV/d at 90°C. The decrease in Tafel slope with increase of temperature has been reported in literature for PtRu/C when the catalyst was incorporated in the MEA with Nafion as electrolyte.[38] Each of the Nyquist plots at 80°C from the impedance spectroscopy of methanol oxidation at different dc potentials shows a capacitive loop in the first quadrant and another pseudoinductive loop in the forth quadrant (Fig. 9). The capacitive loop arises from the charge-transfer resistance of methanol oxidation, and the *x*-axis intercept of the loop represents the magnitude of charge-transfer resistance,[29,39-41] whereas it has been postulated that the presence of the pseudoinductive loop is an indication that the oxidative removal of CO_{ads} is the rate-determining step for methanol oxidation on Pt-Ru at DMFC anodes.[30,42] The improvement in the methanol oxidation kinetics with increasing potential is probably because at higher potentials, Pt sites, beside Ru, supply active oxygen-containing species for CO_{ads} oxidation.[43]

Methanol electro-oxidation on Pt-Ru is an activated process and

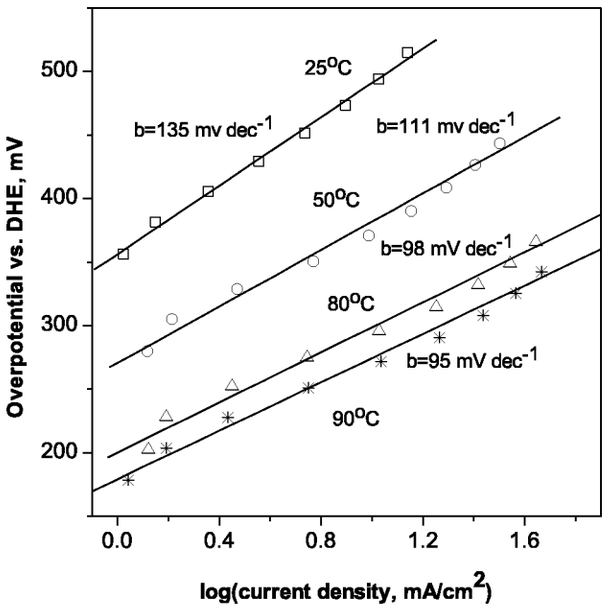

Figure 8. Overpotential vs log(i) at different temperatures for methanol oxidation: 1 mL/min, 1.0 M CH_3OH at the anode, and 5 mL/min humidified H_2 at the cathode. Anode: ~1.5 mg/cm^2 Pt1Ru1. Cathode: ~2 mg/cm^2 20% Pt/Vulcan carbon (E-TEK).

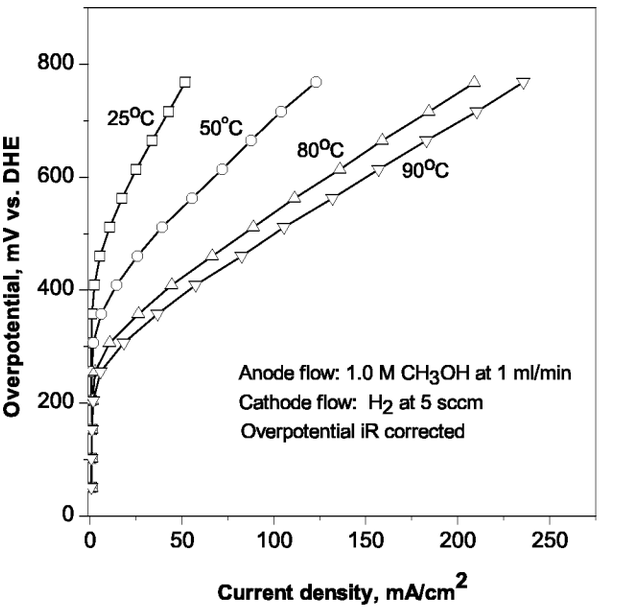

Figure 10. Methanol oxidation overpotential vs current density at different temperatures. Anode: ~1.5 mg/cm^2 Pt1Ru1. Cathode: ~2 mg/cm^2 20% Pt/Vulcan carbon (E-TEK).

depends heavily on temperature.[3] Figure 10 shows the dependence of methanol oxidation on temperature for flame-synthesized Pt-Ru. The onset potential varies from ~400 mV at 25°C to ~250 mV at 90°C. The decrease in the initial activation overpotential with temperature may be because of enhanced hydroxyl species formation on Pt at higher temperature,[43] providing more OH_{ads}-like species for the removal of CO_{ads} or other surface-blocking species. The Nyquist plots at 0.5 V vs DHE show a huge shrinkage of both the first and forth quadrant loops when the temperature is increased from 50 to 80°C at 0.5 V (Fig. 11). This could be an indication of lower charge-transfer resistance of methanol oxidation caused by the improved CO_{ads} oxidation kinetics. An interesting feature in the plot is the temperature dependence of the ohmic resistance, which is given by the interception of the high-frequency curve with the x axis. The ohmic resistance decreases from 1.34 Ω cm^2 at 50°C to 0.96 Ω cm^2 and 0.89 Ω cm^2 at 80 and 90°C, respectively. Arrhenius plots of current density (i) obtained from potentials below 0.5 V are given in

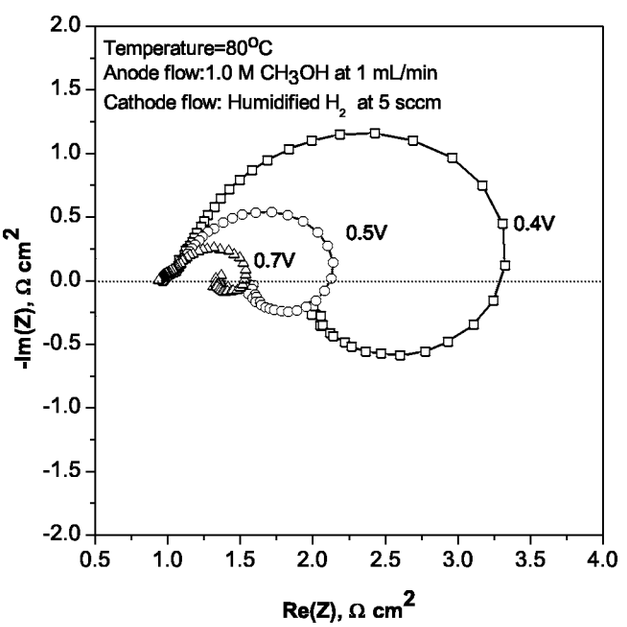

Figure 9. Nyquist plots showing the effect of anode potential vs DHE on the methanol oxidation kinetics at the DMFC anode as determined by impedance spectroscopy. Anode: ~1.5 mg/cm^2 Pt1Ru1. Cathode: ~2 mg/cm^2 20% Pt/Vulcan carbon (E-TEK).

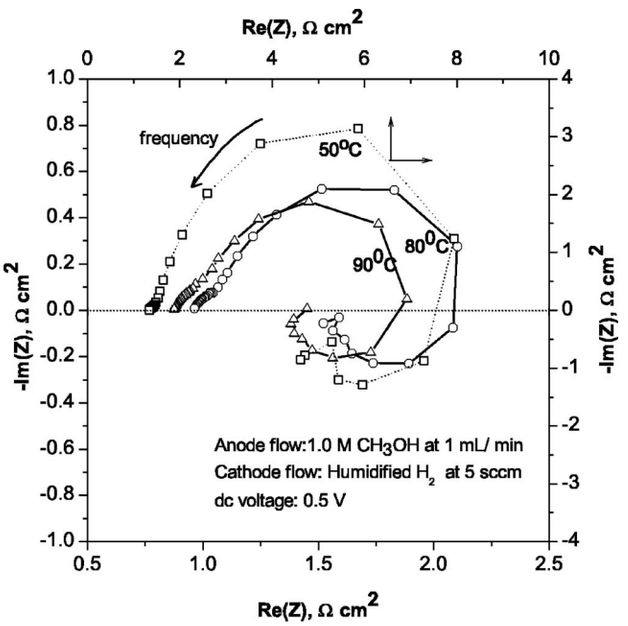

Figure 11. Nyquist plots showing the effect of temperature on methanol oxidation kinetics as determined by impedance spectroscopy at a dc voltage of 0.5 V vs DHE. Anode: ~1.5 mg/cm^2 Pt1Ru1. Cathode: ~2 mg/cm^2 20% Pt/Vulcan carbon (E-TEK).

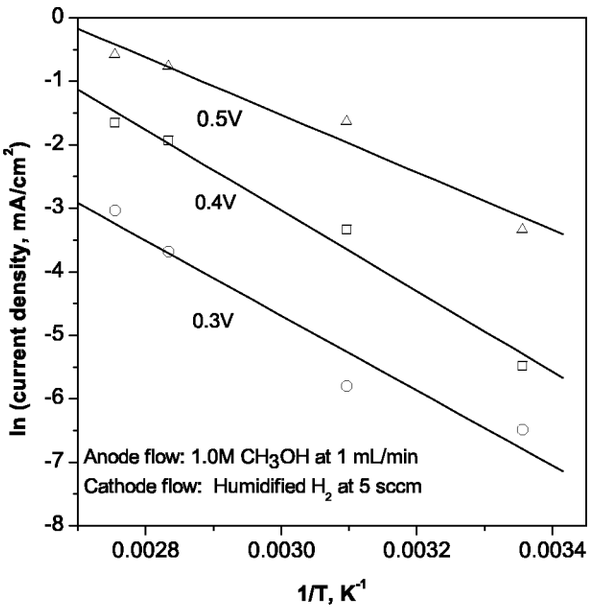

Figure 12. Arrhenius plot at different overpotentials. Anode: ~1.5 mg/cm^2 Pt1Ru1. Cathode: ~2 mg/cm^2 20% Pt/Vulcan carbon (E-TEK).

Fig. 12. The activation energy is 49 kJ/mol at 0.3 V, 53 kJ/mol at 0.4, and 37.6 kJ/mol at 0.5 V. The value at 0.5 V is slightly higher than the 30 kJ/mol reported for PtRu/C obtained at 0.5 V in a genuine fuel cell environment as in this article.[44] However, the average of the three activation energies on our catalyst (47 kJ/mol) is smaller than the average value (58 kJ/mol) below 0.5 V reported on Ru decorated Pt(111)[45] and polycrystalline Pt-Ru (60 kJ/mol).[3,43]

A comparison of performance between flame-synthesized Pt1Ru1 and 1:1 PtRu/C (10% metal loading) is shown in Fig. 13. The supported Pt-Ru catalyst has been chosen for comparison because we wanted to observe the difference between a well-alloyed metallic Pt-Ru catalyst and the flame-synthesized catalyst. The unsupported Pt-Ru has been reported to have lesser degree of alloying and a significant presence of RuO_2 compared to carbon-supported Pt-Ru from E-TEK.[46] The potentials in Fig. 13a have been corrected for iR losses. Even though the onset potentials are similar, the MEA prepared from the flame-synthesized catalyst performs better than the E-TEK catalyst with similar catalyst loading for all higher current densities. At 400 mV, the current density for Pt1Ru1 is ~1.6 times higher than the current density obtained from the MEA with anode made from E-TEK catalyst. For the sake of completeness, we also present the comparison of performance when the fuel cell is producing power, i.e., when O_2 is fed at the cathode and CH_3OH at the anode (Fig. 13b). Again, the performance is better for the MEA that has flame-synthesized Pt1Ru1 anode. It is worthwhile to mention that in this mode of operation, the data obtained could be affected by oxygen reduction kinetics at the cathode and methanol crossover from anode to the cathode, which could be different for two different catalyst layers at the anode.

One has to be careful during comparison of the performance data for catalysts having different physical and chemical properties and prepared by different methods. Besides the difference in the catalytic properties of the active elements, other factors could also affect the performance. The E-TEK Pt1Ru1/C catalyst has a particle size of 2–3 nm, whereas the flame-synthesized Pt1Ru1catalyst has an average particle size of ~10 nm. Because of smaller particle size, the E-TEK catalyst has ~10 times higher specific metal surface area than flame-prepared Pt1Ru1. However, the electrochemically active surface could well be smaller for the anode prepared from the E-TEK catalyst, resulting in the lower current density. Moreover,

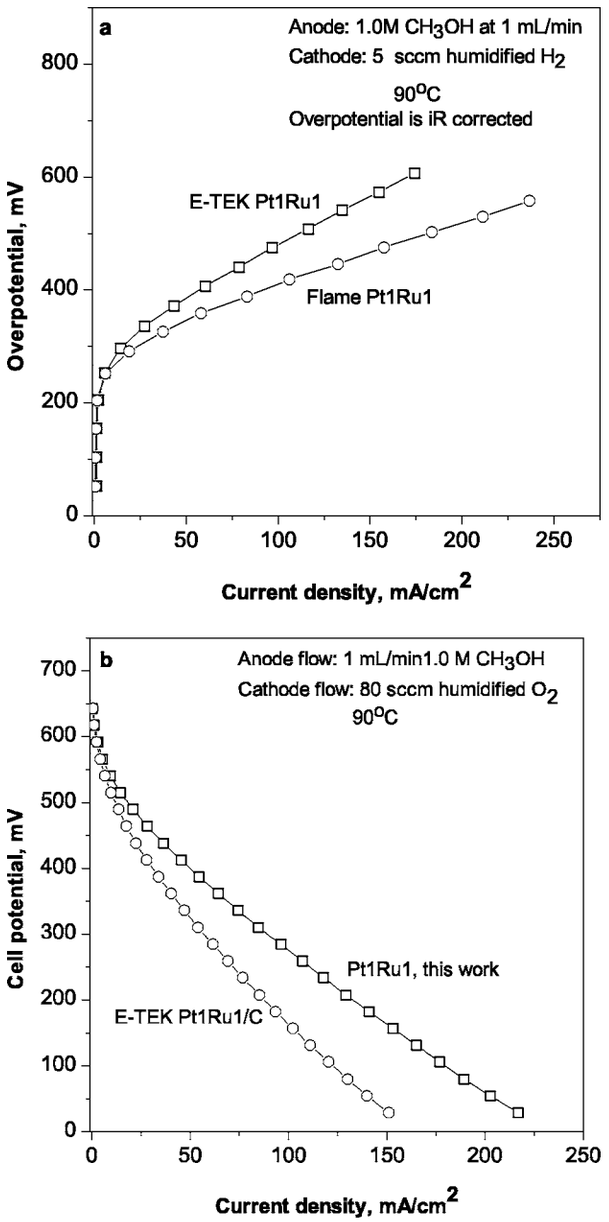

Figure 13. DMFC anode (a) and cell (b) current density–voltage curves, comparing performance of flame-synthesized Pt1Ru1 to that of commercially available E-TEK Pt1Ru1/C as anode catalyst at 90°C. Anode loading: ~1.5 mg/cm^2. Cathode: ~2 mg/cm^2 20% Pt/Vulcan carbon (E-TEK).

the anode catalyst layer prepared from carbon-supported catalyst could have a higher thickness than the unsupported flame-prepared anode, and as a consequence, mass-transfer resistance could be higher in the carbon-supported anode. However, at a low current density, i.e., just above the onset potential, mass-transfer resistance should not have a significant contribution. At an overpotential of 280 mV, the current density obtained from the MEA with anode prepared by E-TEK catalyst is 9 mA/cm^2, whereas that for MEA with anode fabricated from our method is 14 mA/cm^2, i.e., ~1.6 times higher.

XPS data suggest that a significant fraction of Pt and most of the Ru is present as oxides in as-prepared Pt1Ru1 catalyst. However, during conditioning, when the catalyst was exposed to H_2 and subsequently to CH_3OH at 90°C, the metal oxides could be reduced significantly to metallic state.[8] This left us with several possible

speculations about the state of the catalyst after conditioning. Even though there is no bulk alloying, the metals could be partially alloyed at the surface layer. The so-called surface decoration[45,47] of Ru on Pt particles could also be possible. However, with the current results and considering the complexity of the material, we are not in a position to make any definite conclusion about the physical and chemical state of the catalyst at the operating conditions.

Conclusion

We have successfully demonstrated a one-step catalyzation method for preparation of the DMFC anodes. The as-prepared nanocomposites are a mixture of fcc, mostly unalloyed Pt crystalline phase, and an amorphous surface layer, postulated to be a mixture of Pt and Ru oxides. Comparison with commercially available 10%Pt–Ru/C E-TEK catalyst demonstrated that even though the onset potential for methanol oxidation at 90°C on both catalysts are similar (~250 mV), the flame-prepared Pt1Ru1 has 60% higher activity at 0.4 V. However, the exact nature of the physical and chemical state of the flame-synthesized mixed-phase nanocomposite during the methanol oxidation in a fuel cell is yet to be established and is a subject of our ongoing research.

Acknowledgments

This work was supported by PSO (project 5357). The authors wish to thank IRD Fuel Cells A/S for assistance with the project during startup regarding materials and the design of the fuel cell test unit. The scientific and technical support for the EDS analysis of the DG JRC Institute for Energy, Microstructural Analysis Centre, is gratefully acknowledged.

Technical University of Denmark assisted in meeting the publication costs of this article.

References

1. B. D. McNicol, D. A. J. Rand, and K. R. Williams, *J. Power Sources*, **83**, 15 (1999).
2. G. T. Burstein, C. J. Barnett, A. R. Kucernak, and K. R. Williams, *Catal. Today*, **38**, 425 (1997).
3. A. Hamnett, *Catal. Today*, **38**, 445 (1997).
4. T. Frelink, W. Visscher, and J. A. R. van Veen, *Surf. Sci.*, **335**, 353 (1995).
5. M. Watanabe and S. Motoo, *J. Electroanal. Chem. Interfacial Electrochem.*, **60**, 267 (1975).
6. T. Kawaguchi, W. Sugimoto, Y. Murakami, and Y. Takasu, *Electrochem. Commun.*, **6**, 480 (2004).
7. B. Gurau, R. Viswanathan, R. Liu, T. J. Lafrenz, K. L. Ley, E. S. Smotkin, E. Reddington, A. Sapienza, B. C. Chan, T. E. Mallouk, and S. Sarangapani, *J. Phys. Chem.*, **102**, 9997 (1998).
8. H. N. Dinh, X. Ren, F. H. Garzon, P. Zelenay, and S. Gottesfeld, *J. Electroanal. Chem.*, **491**, 222 (2000).
9. S. C. Thomas, X. Ren, and S. Gottesfeld, *J. Electrochem. Soc.*, **146**, 4354 (1999).
10. A. H. C. Sirk, J. M. Hill, S. K. Y. Kung, and V. I. Birss, *J. Phys. Chem. B*, **108**, 689 (2004).
11. J. W. Long, R. M. Stroud, K. E. Swider-Lyons, and D. R. Rolison, *J. Phys. Chem. B*, **104**, 9772 (2000).
12. D. R. Rolison, P. L. Hagans, K. E. Swider, and J. W. Long, *Langmuir*, **15**, 774 (1999).
13. S. J. C. Cleghorn, X. Ren, T. E. Springer, M. S. Wilson, C. Zawodzinski, T. A. Zawodzinski, and S. Gottesfeld, *Int. J. Hydrogen Energy*, **22**, 1137 (1997).
14. W. D. King, J. D. Corn, O. J. Murphy, D. L. Boxall, E. A. Kenik, K. C. Kwiatkowski, S. R. Stock, and C. M. Lukehart, *J. Phys. Chem. B*, **107**, 5467 (2003).
15. R. R. Diaz-Morales, R. Liu, E. Fachini, G. Chen, C. U. Segre, A. Martinez, C. Cabrera, and E. S. Smotkin, *J. Electrochem. Soc.*, **151**, A1314 (2004).
16. S. Hirano, J. Kin, and S. Srinivasan, *Electrochim. Acta*, **42**, 1587 (1997).
17. S. Y. Cha and W. M. Lee, *J. Electrochem. Soc.*, **146**, 4055 (1999).
18. R. O'Hayre, S.-J. Lee, S.-W. Cha, and F. B. Prinz, *J. Power Sources*, **109**, 483 (2002).
19. C. K. Witham, W. Chun, T. I. Valdez, and S. R. Narayanan, *Electrochem. Solid-State Lett.*, **3**, 497 (2000).
20. Y. K. Xiu and N. Nakagawa, *J. Electrochem. Soc.*, **151**, A1483 (2004).
21. E. J. Taylor, E. B. Anderson, and N. R. K. Vilambi, *J. Electrochem. Soc.*, **139**, L45 (1992).
22. S. E. Pratsinis, *Prog. Energy Combust. Sci.*, **24**, 197 (1998).
23. L. Mädler, H. K. Kammler, R. Mueller, and S. E. Pratsinis, *J. Aerosol Sci.*, **33**, 369 (2002).
24. J. P. Hansen, J. R. Jensen, H. Livbjerg, and T. Johannessen, *AIChE J.*, **47**, 2413 (2001).
25. R. W. Cheary and A. A. Coelho, Engineering and Science Research Laboratory, Warrington, England (http://www.ccp14.ac.uk/tutorial/xfit-95/xfit.htm) (1996).
26. C. W. Oatley, *Scanning Electron Microscopy*, p. 187, Cambridge University Press, Cambridge, U.K. (1972).
27. C. D. Wagner, W. M. Riggs, L. E. Davis, and J. F. Moulder, *Handbook of X-Ray Photoelectron Spectroscopy*, G. E. Muilenberg, Editor, p. 22, Perkin-Elmer Corporation, Eden Prairie, MN (1978).
28. C. He, Z. Qi, M. Hollett, and A. Kaufman, *Electrochem. Solid-State Lett.*, **5**, A181 (2002).
29. J. T. Mueller and P. M. Urban, *J. Power Sources*, **75**, 139 (1998).
30. J. T. Müller, P. M. Urban, and W. F. Holderich, *J. Power Sources*, **84**, 157 (1999).
31. H. A. Gasteiger, P. N. Ross, Jr., and E. J. Cairns, *Surf. Sci.*, **293**, 67 (1993).
32. M. C. Denis, G. Lalande, D. Guay, J. P. Dodelet, and R. Schulz, *J. Appl. Electrochem.*, **29**, 951 (1999).
33. A. S. Aricó, P. Cretì, H. Kim, R. Mantegna, N. Giordano, and V. Antonucci, *J. Electrochem. Soc.*, **143**, 3950 (1996).
34. B. J. Kennedy and A. Hamnett, *J. Electroanal. Chem. Interfacial Electrochem.*, **283**, 271 (1990).
35. J. B. Goodenough, A. Hamnett, B. J. Kennedy, and S. A. Weeks, *Electrochim. Acta*, **32**, 1233 (1987).
36. C. Bock, M. A. Blakely, and B. MacDougall, *Electrochim. Acta*, **50**, 2401 (2005).
37. *Practical Surface Analysis by Auger and X-Ray Photoelectron Spectroscopy*, D. Briggs and M. P. Seah, Editors, p. 513, John Wiley & Sons, New York (1983).
38. G. Wu, L. Li, and B. Q. Xu, *Electrochim. Acta*, **50**, 1 (2004).
39. M. Ciureanu, S. D. Mikhailenko, and S. Kaliaguine, *Catal. Today*, **82**, 195 (2003).
40. I.-M. Hsing, X. Wang, and Y.-J. Leng, *J. Electrochem. Soc.*, **149**, A615 (2002).
41. W. Sugimoto, K. Aoyama, T. Kawaguchi, Y. Murakami, and Y. Takasu, *J. Electroanal. Chem.*, **576**, 215 (2005).
42. W. Sugimoto, K. Aoyama, T. Kawaguchi, Y. Murakami, and Y. Takasu, *J. Electroanal. Chem.*, **576**, 215 (2004).
43. H. A. Gasteiger, N. Markovic, P. N. Ross, Jr., and E. J. Cairns, *J. Electrochem. Soc.*, **141**, 1795 (1994).
44. B. Gurau and E. S. Smotkin, *J. Power Sources*, **112**, 339 (2002).
45. G. Tremiliosi-Filho, H. Kim, W. Chrzanowski, A. Wieckowski, B. Grzybowska, and P. Kulesza, *J. Electroanal. Chem.*, **467**, 143 (1999).
46. A. S. Aricó, A. K. Shukla, K. M. El Khatib, P. Cretì, and V. Antonucci, *J. Appl. Electrochem.*, **29**, 671 (1999).
47. P. Waszczuk, J. Solla-Gullon, H.-S. Kim, Y. Y. Tong, V. Montiel, A. Aldaz, and A. Wieckowski, *J. Catal.*, **203**, 1 (2001).